Proceedings of the 17th Czech and Slovak Conference on Magnetism, Košice, Slovakia, June 3–7, 2019

Structural and Magnetic Study of Fe–Al_{20}–(Ti, Nb) Alloys

Y. Jiraskova[a,*], N. Pizurova[a], M. Friak[a] and D. Janickovic[b]

[a]Institute of Physics of Materials, Academy of Sciences of the Czech Republic, Žižkova 22, 616 62 Brno, Czech Republic

[b]Institute of Physics, Slovak Academy of Sciences, Dubravska cesta 9, 845 11 Bratislava, Slovakia

The present studies are devoted to a set of $Fe_{80}Al$-based alloys in which Fe atoms are substituted by Ti (5 at.% or 8 at.%), and by 4 at.% Ti + 4 at.% Nb. The Mössbauer and magnetic observations are supported by chemical and structural analysis using scanning and transmission electron microscopy (TEM), and X-ray diffraction. The chemical compositions at all samples turn out to be in good agreement with the nominal one regardless investigated area, but certain differences are detected at sample containing Nb. In the sample modified by Ti+Nb, coherent precipitates uniformly distributed in Fe–Al-based matrix are identified by TEM. Regarding macroscopic magnetic properties the saturation magnetization decreases with increasing Ti content, however, a partial substitution of Ti by Nb evokes an opposite effect, i.e., an increase of the saturation magnetization by 87.5%. All ternary and quaternary alloys yield a higher temperature stability of magnetic properties as compare to the parent $Fe_{80}Al_{20}$. The Mössbauer results confirm the dominant ferromagnetic phase and the accompanied paramagnetic phase. Their relative amounts depend on the Ti and Nb alloying. The changes in magnetic microstructure are reflected in hyperfine parameters.

DOI: 10.12693/APhysPolA.137.835

PACS/topics: Fe–Al–(Ti,Nb) alloys, structure, magnetic properties

1. Introduction

The Fe-Al based alloys in concentration range of Al between 20 at.% and 25 at.% are still frequently studied experimentally, as well as theoretically [1–3]. They exhibit good oxidation resistance, high strength and predominantly low cost. Their modification by third element, e.g., as Ti, Mo, Nb, Zr, Cr, receives considerable attention presently motivated by the search for high temperature structural materials. Some of these alloying elements aim at increasing the strength by different mechanisms, e.g., as solid solution precipitates, and short- or long-range ordering strengthening [4]. The effects of ternary additions on the ordering phenomena are studied predominantly from viewpoint of structure and mechanical properties. Studies of the Fe–Al system modified by Ti show that a two-phase equilibrium between disordered A2 and $L2_1$ ordered Fe_2TiAl can exist [5, 6] if the difference of lattice constants is sufficiently small and coherent A2+$L2_1$ microstructures are formed [4]. Aligned/coherent two-phase microstructures with A2, B2, $D0_3$ or $L2_1$, were reported also in other Fe–Al-ternary compositions, e.g., with Ta [7] or Nb [8, 9]. Similarly as in a case of Ti addition, the studies concerning Nb addition are mainly devoted to strengthening of Fe–Al alloys. The present work reports the results of investigation of the structure formed in Fe-20 at.% Al system with Fe substituted by Ti, and newly by combination of Ti and Nb. The previous studies were devoted to mechanical properties [10] and to theoretical calculations of Fe-Al system [11]. This work continues the recent studies of the Fe-22 at.% Al-7 at.% Ti system [12].

2. Experimental details

The arc melted button-type alloys were prepared from high-purity elements, i.e., Fe(99.95%), Ti(99.8%), Al(99.95%), Nb(99.8%), using a MAM-1 furnace (Buehler GmbH), and re-melted four times under Ar (4N8) of 35 kPa pressure to guarantee a good chemical homogeneity. Subsequently, the samples were prepared according to requirements of experimental methods and studied in their as-prepared states. They were denoted FA ($Fe_{80}Al_{20}$), FAT5 ($Fe_{75}Al_{20}Ti_5$), FAT8 ($Fe_{72}Al_{20}Ti_8$) and FATN ($Fe_{72}Al_{20}Ti_4Nb_4$).

A TESCAN LYRA 3XMU FEG/SEM scanning electron microscope working at accelerating voltage of 20 kV equipped with an XMax80 Oxford Instruments detector for energy dispersive X-ray analysis (EDX) was used to follow the chemical composition. A Jeol JEM 2100F HRTEM with a Schottky cathode operating at 200 kV was applied for microstructural details.

An X'PERT PRO diffractometer (Panalytical) in the Bragg-Brentano geometry with CoK_α radiation ($\lambda = 0.17902$ nm) was used for measurements at room temperature (RT) in the range of 2Θ from 35° to 135° in steps of 0.01° and 500 s/° using spin mode. The analysis of patterns was realized by HighScore Plus program using the Rietveld structure refinement method [13], and the ICSD database [14].

RT hysteresis loops and thermomagnetic curves (TMC) in an external field of 400 kA/m, vacuum, and temperature increase 4 K/min, were measured using

*corresponding author; e-mail: jirasko@ipm.cz

a vibrating sample magnetometer EG&G Princeton Applied Research Corporation. The coercivity, remanent and saturation magnetizations were derived from the hysteresis loops with accuracy of ±1%.

The ^{57}Fe Mössbauer measurements were carried out at RT using a ^{57}Co(Rh) source in scattering geometry by detecting γ-rays with depth sensitivity of ~ 30 μm. The calibration of velocity scales was performed with α-Fe and the isomer shifts are given with respect to the RT Mössbauer spectrum of α-Fe. All spectra were evaluated within the transmission integral approach using the CONFIT program package [15]. In the measured spectra the paramagnetic (pm) components are represented by discrete single- and double-line Lorentzian subspectra determined by discrete values of isomer shift(s) δ, and quadrupole splitting(s) Δ. The ferromagnetic (fm) components are in addition represented by hyperfine induction(s) B. All components are further described by their relative intensities A.

3. Results and discussion

The morphologies of the pure $Fe_{80}Al_{20}$ (FA) and both Ti containing samples (FAT5, FAT8) are very similar, and they are represented by the $Fe_{75}Al_{20}Ti_5$ sample in Fig. 1a. A different structure was observed at the sample containing Ti+Nb (FATN) as clearly seen in Fig. 1b. The EDX element analysis taken from an area of approximately 0.1 mm^2 does not reveal any important differences in composition compared to the nominal. On the other hand, the more detailed analysis of black and white areas at the FATN sample yields an inhomogeneous composition. All results are summarized in Table I.

The XRD pattern analysis has shown that about 60% of the FA sample is ordered into $D0_3$ structure with lattice parameter $a = 0.5808$ nm and into residual bcc A2 structure ($a = 0.2907$ nm). Both results are in good agreement with, e.g., Buschow et al. [16]. The 5 at.% Ti addition has changed the pattern but only one phase of lattice parameter $a = 0.5805$ nm agreeed with that presented for Fe_3Al phase [16]. Nevertheless, the Mössbauer measurements presented below document two phase composition (Fig. 2). The sample with 8 at.% Ti consists of A2 and $D0_3$ phases of lattice parameters 0.2911 nm and 0.5803 nm, respectively. Different microstructure, similar to those obtained for Fe–26Al–4Nb [17],

TABLE I

The EDX element analysis from 0.1 mm^2 area.

Sample	Fe	Al	Ti	Nb
	[at. %]			
FA ($Fe_{80}Al_{20}$)	80.1	19.9	–	–
FAT5 ($Fe_{75}Al_{20}Ti_5$)	73.6	21.4	5.0	–
FAT8 ($Fe_{72}Al_{20}Ti_8$)	71.9	20.1	8.0	–
FATN ($Fe_{72}Al_{20}Ti_4Nb_4$)	70.4	19.8	4.1	5.7
black area	74.3	20.8	3.3	1.6
white area	67.0	17.3	5.3	10.4

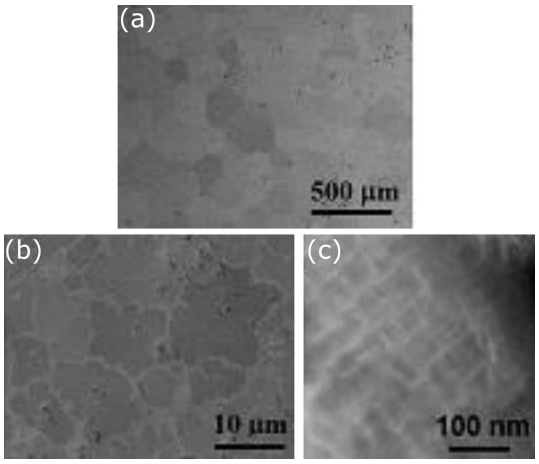

Fig. 1. SEM micrographs of (a) $Fe_{75}Al_{20}Ti_5$ (FAT5), (b) $Fe_{72}Al_{20}Ti_4Nb_4$ (FATN), and (c) TEM micrograph of FATN sample.

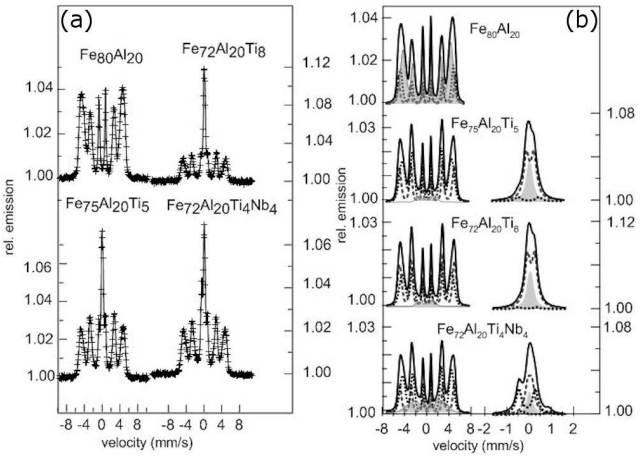

Fig. 2. Mössbauer spectra (a), and (b) the decomposition into ferromagnetic and paramagnetic components.

and more complicated phase composition were detected at the sample with Ti+Nb addition. The black areas feature higher content of Fe at the expense of mainly Nb while the white ones are abundant in Nb and have lower Fe and Al contents. The analysis of XRD pattern yields besides bcc A2 phase ($a = 0.2908$ nm), the bcc-Fe_2TiAl phase, $a = 0.5846$ nm, similar to value presented in [12], and hexagonal Fe_2NbAl phase of parameters $a = 0.4844$ nm and $c = 0.7881$ nm. The first TEM observations of the FATN lamella taken probably from the black area document a presence of grains of the size about (45–50) nm similar to cuboids observed in [12]. Their mean composition is 73.3 at.% Fe, 21.6 at.% Al, 3.2 at.% Ti, and 1.9 at.% Nb.

From the viewpoint of magnetic behaviour the Ti addition decreases the saturation magnetization M_S compared to pure FA alloy, while the Ti+Nb evokes an opposite effect. The analysis of RT hysteresis loops after TMC (RT-1000K-RT) has yielded practi-

TABLE II

Saturation, M_S, and remanent, M_r, magnetizations and coercivity, H_c, derived from the hysteresis curves prior (1) and after (2) TMC measurements at room temperature and the Curie temperature T_C.

Sample	FA	FAT5	FAT8	FATN
M_{s1} [A m^2/kg]	146.9	121.3	95.7	180.1
M_{s2} [A m^2/kg]	162.0	120.6	95.7	179.6
M_{r1} [A m^2/kg]	0.5	4.0	9.6	1.3
M_{r2} [A m^2/kg]	0.4	4.7	6.7	0.9
H_{c1} [kA/m]	0.5	3.8	9.9	0.9
H_{c2} [kA/m]	0.4	4.5	6.8	0.7
T_C [K]	944	948	962	944

TABLE III

Ferromagnetic phase: mean values of hyperfine inductions B, isomer shift δ, quadrupole splitting Δ, and relative representation of components A, obtained from the spectra analysis.

	DHB1	DHB2	DHB3
FA $Fe_{80}Al_{20}$			
B [T]	31.9	29.6	26.6
δ [mm/s]	0.021	0.035	0.033
Δ	−0.009	−0.009	0.009
A [%]	16.7	25.5	57.8
FAT5 $Fe_{75}Al_{20}Ti_5$			
B [T]	30.8	27.6	10.9
δ [mm/s]	0.006	0.017	−0.027
Δ	0.008	0.011	0.053
A [%]	26.3	45.1	3.9
FAT8 $Fe_{72}Al_{20}Ti_8$			
B [T]	30.7	27.7	9.8
δ [mm/s]	0.06	0.041	−0.049
Δ	0.009	0.014	−0.143
A [%]	29.7	29.6	2.9
FATN $Fe_{72}Al_{20}Ti_4Nb_4$			
B [T]	30.7	27.5	20.1
δ [mm/s]	0.068	0.06	0.1
Δ	0.005	0.01	−0.018
A [%]	19.7	36.8	14.8

cally the same M_S values of the alloyed samples, documented the higher temperature stability of magnetic properties (Table II). However, a huge increase in M_S after replacing 4 at.% Ti by 4 at.% Nb is not fully clear. The first theoretical calculation done for disordered FA, FAT8, and FATN samples allow us to obtain their magnetic moments of 1.77 μ_B/atom, 1.43 μ_B/atom, and 1.44 μ_B/atom, respectively. This results confirm a decrease of magnetic moment due to Ti addition but no distinct increase in M_S with partial substitution of Ti by Nb. This aspect remains unclear and open for the next studies.

TABLE IV

Paramagnetic phase: mean values of isomer shift δ, quadrupole splitting Δ, and relative representation of components A, obtained from the spectra analysis.

	D1	D2	D3	L
FAT5 $Fe_{75}Al_{20}Ti_5$				
δ [mm/s]	0.043	−0.035	–	0.011
Δ	0.334	0.942	–	–
A [%]	16.1	1.5	–	7.0
FAT8 $Fe_{72}Al_{20}Ti_8$				
δ [mm/s]	0.086	−0.083	–	0.048
Δ	0.318	0.803	–	–
A [%]	26.7	1.0	–	10.1
FATN $Fe_{72}Al_{20}Ti_4Nb_4$				
δ [mm/s]	0.030	−0.098	0.278	0.018
Δ	0.182	0.740	1.216	–
A [%]	11.4	10.8	1.7	4.8

The Mössbauer spectra of all samples are shown in Fig. 2a. Figure 2b represents the ferromagnetic and paramagnetic contributions separately. The best fit of the fm phase was obtained using three distributions of hyperfine inductions (DHB), and the pm phase was analyzed by doublets (D) and a singlet (L). The mean values of hyperfine parameters and their relative representations are summarized in Tables III and IV.

According to Athanassiadis observations the pm components are visible in the RT Mössbauer spectra for the Ti addition above 3 at.% [18]. In the present case, the Ti addition increases the pm contribution from 24.6 % (FAT5) to 37.8 % (FAT8), however, the Nb addition at the expense of Ti supports rather the fm phase. The pm phase is probably Fe_2TiAl detected also by XRD. The more detailed analysis of Mössbauer data is also open for next studies.

4. Conclusions

Present investigations are devoted to the structural and physical properties of the parent Fe-20 at.% Al alloy modified by Ti and Nb at the expense of Fe. The studies have shown that Ti addition decreases the saturation magnetization whereas Nb yielded an opposite effect. The Ti+Nb addition resulted in a different microstructure compared to the alloys with only Ti addition. Several unclear effects following from the magnetic and Mössbauer results, mainly the huge increase in saturation magnetization of the sample with 4 at.% Ti + 4 at.% Nb compared to sample with 8 at.% Ti (87.5%) are unresolved, and remain for the next experimental and theoretical investigations. The first theoretical calculations of disordered solid solutions have confirmed the decreasing tendency of saturation magnetization due to Ti addition but not its increase due to partial substitution of Ti by Nb.

Acknowledgments

This work was supported by the projects, 17-22139S funded by the Czech Science Foundation and VEGA 2/0082/17 funded by the SRDA. Special thanks are given to M. Hapla and I. Turek from IPM Brno for the magnetic measurements and fruitful discussions.

References

[1] C.H. Sellers, T.A. Hyde T.K. O'Brien R.N. Wright, *J. Phys. Chem. Solids* **565**, 505 (1994).

[2] P. Šesták, M. Friak, D. Holec, M. Vsianska, M. Sob, *Nanomaterials* **8**, 873 (2018).

[3] M. Friák, S. Oweisova, J. Pavlu, D. Holec, M. Sob, *Materials* **11**, 1543 (2018).

[4] M. Palm, *Intermetallics* **13**, 1286 (2005).

[5] M. Palm, J. Lacaze, *Intermetallics* **14**, 1291 (2006).

[6] M. Palm, G. Inden, N. Thomas, *J. Phase Equilib.* **16**, 209 (1995).

[7] M. Palm, R. Krein, S. Milenkovic, G. Sauthoff, D. Risanti, C. Stallybrass, A. Schneider, *MRS Proc.* **980**, II01-01 (2007).

[8] D.M. Dimiduk, M.G. Mendiratta, D. Banerjee, H.A. Lipsitt, *Acta Metall.* **36**, 2947 (1988).

[9] D.G. Morris, L.M. Requejo, M.A. Munos-Morris, *Intermetallics* **13**, 862 (2005).

[10] P. Dymacek, F. Dobes, Y. Jiraskova, N. Pizurova, M. Friak, *Theor. Appl. Fract. Mechan.* **99**, 18 (2019).

[11] I. Mihalikova, M. Friak, Y. Jiraskova, D. Holec, N. Koutna, M. Sob, *Nanomaterials* **8**, 1059 (2018).

[12] Y. Jiraskova, N. Pizurova, A. Titov, D. Janickovic, M. Friak, *J. Magn. Magn. Mater.* **468**, 91 (2018).

[13] R.A. Young *The Rietveld Method* International Union of Crystallography, Oxford University Press, Oxford 1993.

[14] ICSD Database, Version 1.9.4., 2014-1, NIST/FIZ.

[15] T. Zak, Y. Jiraskova, *Surf. Interface Anal.* **38**, 710 (2006).

[16] K.H.J. Buschow, P.G. van Engen, R. Jongebreur, *J. Magn. Magn. Mater.* **38**, 1 (1983).

[17] F. Stein, C. He, O. Prymak, S. Voss, I. Wossack, *Intermetallics* **59**, 43 (2015).

[18] G. Athanassiadis, G. LeCaer, J. Foct, L. Rimlinger, *Phys. Stat. Sol. a* **40**, 425 (1977).